(Running title:) Aldolase microcompartmentation in Arabidopsis guard cells

(Title:) Microcompartmentation of cytosolic aldolase in Arabidopsis by interaction with the actin cytoskeleton

Constantine Garagounis[1,4], Kalliopi-Ioanna Kostaki[2], Tim J. Hawkins[3], Ian Cummins[3], Mark D. Fricker[1], Patrick J. Hussey[3], Alistair M. Hetherington[2] and Lee J. Sweetlove[1]

[1]Department of Plant Sciences, University of Oxford, South Parks Road, Oxford OX1 3RB, UK

[2]School of Biological Sciences, University of Bristol, Life Sciences Building, 24 Tyndall Avenue, Bristol BS8 1TQ, UK

[3]School of Biosciences, Durham University, South Road, Durham, DH1 3LE, UK

[4]Corresponding author: kgkaragkounis@bio.uth.gr;

Highlight:

Microcompartmentation is a form of cellular organisation caused by the interaction of proteins with cellular structures and endomembranes. We show that a cytosolic isozyme of the enzyme aldolase is microcompartmented in Arabidopsis guard cells by interaction with the actin cytoskeleton.

Abstract

Evidence is accumulating for molecular microcompartments formed when proteins interact in localised domains with the cytoskeleton, organelle surfaces, and intracellular membranes. To understand the potential functional significance of protein microcompartmentation in plants, we studied the interaction of the glycolytic enzyme fructose bisphosphate aldolase with actin in *Arabidopsis thaliana*. Homology modeling of a major cytosolic isozyme of aldolase, FBA8, suggested that the tetrameric holoenzyme has two actin binding sites and could

therefore act as an actin-bundling protein, as was reported for animal aldolases. This was confirmed by *in vitro* measurements of an increase in viscosity of F-actin polymerized in the presence of recombinant FBA8. Simultaneously, interaction with F-actin caused non-competitive inhibition of aldolase activity. We did not detect co-localisation of an FBA8-RFP fusion protein, expressed in an *fba8*-knockout background, with the actin cytoskeleton using confocal laser-scanning microscopy. However, we did find evidence for a low level of interaction using FRET-FLIM analysis of FBA8-RFP co-expressed with the actin-binding protein GFP-Lifeact. Furthermore, knockout of FBA8 caused minor alterations of guard cell actin cytoskeleton morphology and resulted in a reduced rate of stomatal closure in response to decreased humidity. We conclude that cytosolic aldolase can be microcompartmented *in vivo* by interaction with the actin cytoskeleton and may subtly modulate guard cell behavior as a result.

Keywords: actin-binding, actin-bundling, aldolase, co-localisation, guard cell actin, guard cell metabolism, microcompartmentation;

Abbreviations list: ABA: abscisic acid, CLSM: confocal laser-scanning microscopy, FBA**:** fructose bisphosphate aldolase, F1,6-BP: fructose 1,6-bisphosphate, FRET-FLIM: Forster resonance energy transfer-fluorescence lifetime imaging microscopy, ROI: region of interest;

Introduction

Microcompartmentation is the phenomenon where soluble proteins have a non-homogeneous distribution within a single, membrane-bounded, sub-cellular compartment, typically through interaction of proteins with intracellular membranes or other cellular structures such as the cytoskeleton (Hudder *et al.*, 2003; Gierasch and Gershenson, 2009) and through liquid phase separation (Feric *et al.*, 2016). It remains unclear how this higher-level organization affects cell function, but there is some evidence that dynamic microcompartmentation plays a regulatory role in both metabolism and intracellular signaling (Sweetlove

and Fernie, 2013). For example, glycerol phosphate dehydrogenase and various glycolytic enzymes, including aldolase, locate to actin-rich regions of the cell in fly muscle. Knocking out this muscle-specific isozyme of glycerol phosphate dehydrogenase led to a flightless fly phenotype and also caused glycolytic enzymes to become uniformly distributed (Wojtas *et al.*, 1997; Sullivan, 2003). In HeLa cells, enzymes involved in the synthesis of purines co-localized in distinct punctate bodies, which were themselves co-localized with the microtubule cytoskeleton when cells were grown on purine-depleted media, but had a uniform cytosolic distribution when cells were grown in the presence of exogenous purines (An *et al.*, 2008; An *et al.*, 2010). Both these examples illustrate how specific metabolic pathways may be rapidly modulated via reversible enzyme microcompartmentation. Additionally, recent theoretical models suggest that microcompartmentation of enzymes by association with the tubulin cytoskeleton may be used to integrate various metabolic pathways with other ongoing cellular processes, thereby linking metabolic regulation with the current cell status (Olah *et al.*, 2015).

In plants there are several known instances of microcompartmentation of enzymes, including association of enzymes with microtubules (Chuong *et al.*, 2004) and actin (Holtgrawe *et al.*, 2005; Wojtera-Kwiczor *et al.*, 2012), association of glycolytic enzymes with the surface of organelles (Giege *et al.*, 2003; Balasubramanian *et al.*, 2007; Graham *et al.*, 2007; Huang *et al.*, 2009) or other intracellular membranes (Barkla *et al.*, 2009), and association of enzymes of secondary metabolism with the cytosolic face of the ER (Hrazdina and Wagner, 1985; Moller, 2010). In several of these examples, a role in metabolic regulation has been suggested, either through the facilitation of metabolite channeling between sequential enzymes (Graham *et al.*, 2007) or by controlling reaction products of low-specificity enzymes (Moller, 2010).

To further investigate the role of enzyme microcompartmentation in plants, we analysed the localization of a cytosolic isozyme, AtFBA8 (encoded by the *At3g52930* gene), of the glycolytic enzyme aldolase in Arabidopsis. Aldolase (EC 4.1.2.13) is the fourth enzyme of the Embden-Meyerhof-Parnas glycolytic

pathway and mediates cleavage of fructose 1,6-bisphosphate (F1,6-BP) into glyceraldehyde 3-phosphate and dihydroxyacetone phosphate. AtFBA8 is the most abundantly expressed of four cytosolic aldolase isozymes in Arabidopsis according to publicly available microarray data (Hruz *et al.*, 2008), there are also four plastidic aldolase isozymes in (Graham, 2007). Previous work has provided *in vitro* evidence showing aldolase is able to associate with the mitochondrial surface in Arabidopsis cell cultures and potato tubers (Giege *et al.*, 2003; Graham *et al.*, 2007), to interact with actin in yeast-two-hybrid experiments and co-sedimentation assays (Holtgrawe *et al.*, 2005; Wojtera-Kwiczor *et al.*, 2012), and to co-immunoprecipitate with actin when using an anti-aldolase antibody (Graham, 2007). However, the functional significance of the aldolase-actin interaction has not been determined. Thus, we first investigated the interaction of aldolase FBA8 with actin *in vitro* to assess potential reciprocal functional effects that these two proteins might exert on each other. We then assessed the occurrence of aldolase microcompartmentation with actin *in vivo* using microscopy and finally determined potential functions of this interaction using genetic approaches.

Materials and Methods

Aldolase sequence alignment and structural modeling

The aldolase *At3g52930* sequence was retrieved from the TAIR database. Human (PAN P04075) and rabbit muscle (PAN P00883) aldolase protein sequences and actin sequences P68133 and P68135 from human and rabbit muscle, respectively, were aligned using Clustal Omega and LALIGN on the EMBL website (ebi.ac.uk). Homology modeling was carried out using the Swiss-PdbViewer DeepView, version 4.0.1, (Guex and Peitisch, 1997). The crystal structure of rabbit muscle aldolase (RCSB PDB reference: 3DFQ) was used as a template and the resulting model structure of Arabidopsis aldolase FBA8 was modified in RasMol (Sayle and Milner-White, 1995) to mark residues of interest.

Reagents and plant growth conditions used

Chemicals and enzymes were purchased from Sigma Aldrich (St. Luis, MO, USA). Rabbit muscle actin (catalogue number AKL99) was purchased from

Denver Cytoskeleton Inc. (Denver, CO, USA). *Arabidopsis thaliana* ecotype Columbia-0 (Col-0) was used as a wild type control and was the basic genetic background for all other plant lines used in this work. Salk T-DNA insertion lines for FBA8:, Salk_124383 (*fba8-1)*, SALK_058908 (*fba8-2*), and SALK_007216 (*fba8-3*)*)* were ordered from the Nottingham Arabidopsis Stock Centre (NASC). Unless specified otherwise, plants were germinated and grown on 0.8% (w/v) agar plates supplemented with half-strength Murashige-Skoog (MS) salts (Duchefa Biochemie, Haarlem, Netherlands) and 1% (w/v) sucrose for up to 10 days before transfer to 3:1 (v/v) compost:vermiculite mixture. Growth conditions were 16/8hrs, light/dark at 22-23^{o}C. *Nicotiana tabacum* cultivar "Little Havana" and *Nicotiana benthamiana* were grown at 25^{o}C 16/8hrs, light/dark on 3:1 (v/v) compost:vermiculite.

Nucleic acid extraction and PCR conditions

Genomic DNA from Arabidopsis tissues was extracted by grinding tissue under liquid N_2, adding DNA-extraction buffer [200mM Tris-HCl pH7.5, 250mM NaCl, 25mM ethylene-diamine tetra-acetic acid, (EDTA) and 0.5% (w/v) sodium-dodecyl sulfate (SDS)] followed by isopropanol precipitation. DNA concentration was measured by Nanodrop (Thermo Fischer). RNA was extracted from mature Arabidopsis leaves using the TRIzol® reagent from (Life Technologies, Thermo-Fischer) following the manufacturer's instructions. Resulting RNA was treated with DNase I (Fermentas). Reverse transcription of DNase-treated RNA was carried out using the M-MLV reverse transcription kit and protocol from Sigma-Aldrich with an oligo-deoxythymidine primer. PCRs on resulting cDNA were carried out as described below with primers targeting a fragment of the ubiquitin-10 transcript and the full-length aldolase FBA8 (At3g52930) transcript (Supplementary Table S1).

PCR was carried out using Megamix Blue (Microzone Ltd., UK) according to the manufacturers instructions (Supplementary Table 1 for primer pairs and annealing temperatures). PCRs for sub-cloning of the aldolase coding sequence (CDS) were carried out using Phusion High-Fidelity DNA polymerase (Thermo-Fischer, Waltham, MA, USA). The RFP CDS was PCR-amplified from the

pUB:GW:RFP vector (Grefen *et al.*, 2010). For expression in *Pichia pastoris,* the aldolase CDS was sub-cloned into the expression vector, pPICZαB (Invitrogen, Carlsbad, CA, USA) using the PstI and XbaI restriction sites. The FBA8 CDS was cloned in frame with the N-terminal secretion peptide and included a stop codon. For expression of aldolase in plant cells, the aldolase CDS was sub-cloned into binary vectors pUB:GW:RFP and pUB:RFP:GW described in (Grefen *et al.*, 2010) to generate N- and C-terminal fusions of aldolase with mRFP1. The free RFP CDS was cloned into the pUB:GW vector (Grefen *et al.*, 2010). Orientation and sequence of the inserts in all of the generated plasmids was verified by restriction digest and DNA sequencing. The GFP:Lifeact (GFP6) construct was made in the pMDC43 binary vector (Deeks *et al.*, 2010). The free GFP (roGFP2) construct (Schwarzlander *et al.*, 2009) was donated by Dr. Markus Schwarzlander (University of Bonn, Germany).

Recombinant expression and partial purification of *At*FBA8 from *Pichia pastoris*

Wild type *Pichia pastoris* strain X-33 was transformed with the empty pPICZalphaB plasmid and with the aldolase constructs and mutant variants cloned in pPICZalphaB using the electroporation protocol described in the Easy Select™ Pichia expression kit manual from Invitrogen (Life Technologies). Methanol induced expression of aldolase variants was carried out in 100 or 500mL cultures of the resulting strains as described in this manual using the BMGY and BMMY media described therein. Clarified culture media (Pichia cells removed by centrifugation 1,500 x *g* for 10min at 4^{o}C) was assayed for aldolase enzyme activity, or analysed by SDS-PAGE and western blotting with an anti-aldolase antibody in order to verify presence of the recombinant protein. Un-tagged aldolase was partially purified from media of expressing cultures using $(NH_4)_2SO_4$ fractionation. Clarified media was chilled to 4^{o}C in glass conical flasks. $(NH_4)_2SO_{4(s)}$ was added initially to 35% (w/v) and mixed with a stirrer bar for 1hr. This solution was centrifuged for 15min at 10,000 x *g.* The resulting 35% pellet fraction was kept on ice. More $(NH_4)_2SO_{4(s)}$ was added to the remaining supernatant fraction to 65% saturation and the procedure above was repeated. All of the steps were carried out at 4^{o}C. 35% and 35-65% $(NH_4)_2SO_4$ pellet

fractions were re-suspended in 1mL final buffer (see below) and desalted using Zeba desalting columns (Thermo-Fischer, product code 89877) as described in the manufacturer's manual and further analysed for aldolase enzyme activity and total protein content (Supplementary Table S2 and Fig. S1). The final buffer for aldolase desalting and storage was [25mM HEPES-NaOH pH 7.0, 2mM $MgCl_2$, 1mM EDTA, 0.2mM EGTA, 1mM DTT, 20% (v/v) ethylene glycol] adapted from (Moorhead *et al.*, 1994).

Arabidopsis crude protein extraction and aldolase activity assays

Arabidopsis total soluble protein was extracted by grinding tissues to a fine powder under liquid N_2 with a pre-chilled (-20°C) mortar and pestle. A volume of extraction buffer [50mM Tris-HCl pH 7.4, 10% (v/v) glycerol, 0.1% (v/v) Triton-X100, 1mM EDTA, 1mM DTT, 1mM phenylmethylsulfonyl-fluoride (PMSF), 5% (w/v) poly-vinyl-polypyrrolidone (PVPP)] was added at a ratio of 1µLmg^{-1} of tissue. Samples were then centrifuged at 12,000 x *g* for 10min at 4°C. The resulting supernatant represented the total soluble protein crude extract. and further analyzed by enzyme activity assays or by SDS-PAGE and western blotting.

Enzyme activity assays were carried out at 340nm in 1.5mL plastic cuvettes or 96-well plates using a Unicam UV/Vis, model UV4, spectrophotometer, or a Beckman-Coulter DTX 880 Multimode Detector plate-reader, respectively. Spectrophotometer assays were in a final volume of 1mL and plate reader assays were carried out in a 200µL volume according to (Graham, 2007). To measure aldolase activity in the presence of polymerised actin, aldolase was added to actin, or BSA-containing samples in low salt buffer (LSB, 5mM Tris-Cl pH8.0, 0.2mM $CaCl_2$, 0.2mM ATP, 0.5mM DTT). Polymerisation was induced by addition of 10xPIB (500mM KCl, 20mM $MgCl_2$, 10mM ATP) to a 1x concentration. Samples were allowed to polymerise for 1hr at room temperature and then a mix of Hepes-NaOH pH7.7, NADH, TPI, G3PDH and F1,6BP was added to the same final concentrations as above in a final reaction volume of 200µL. In non-polymerised actin control samples an equivalent volume of LSB was added instead of 10xPIB. For each sample assayed, a control

sample without F1,6BP was also measured to control for background NADH oxidation. One unit was defined as a substrate conversion rate of 1µmol min^{-1}. Kinetic parameters were calculated using the Solver add-in of Microsoft Office's Excel. A hyperbolic curve described by the Michaelis-Menten equation using random initial parameters was best-fit to experimental data by minimizing the sum-of squared distances for each data-point from the fitted line.

Proteins separated by SDS-PAGE were Coomassie-stained, or transferred to nitrocellulose membranes for western blotting. Ponceau S staining was used to monitor protein transfer and equal sample loading. Aldolase was detected using an anti-cytosolic aldolase, rabbit, primary antibody, described in (Moorhead *et al.*, 1994), and an anti-rabbit antibody conjugated with horseradish peroxidase was used for detection with a WestPico ECL chemiluminescence kit (Thermo-Fischer) following this manufacturer's instructions. Protein concentrations were measured using Bradford's Quick StartTM reagent from Bio-Rad (Hercules, CA, USA) and a BSA standard curve. Densitometric analysis of gel and blot images was conducted using FIJI (Schindelin *et al.*, 2012).

Aldolase-actin interaction *in vitro* assays

Co-sedimentation assays with actin (Denver Cytoskeleton Inc. Denver, CO, USA) were carried out using purified rabbit muscle actin as described in the corresponding datasheet and using the amounts of actin and test proteins (aldolase, or BSA) specified in each experiment in 500µL, or 1mL final sample volumes. All proteins were buffer exchanged into LSB prior to use. Centrifugation steps were carried out at 100,000g for 1 hour at 25°C. Serial co-sedimentation was carried out as above, but conducted at low speed (13,000 x *g* for 30min at 25°C) to pellet bundled F-actin. Equivalent amounts of each fraction (after pellet re-suspension in LSB) were analysed by SDS-PAGE and or Bradford assay.

For actin polymerisation assays, purified actin suspended in LSB at a concentration of 10mgmL^{-1} was spiked with pyrene-labeled actin (Denver Cytoskeleton Inc.) to 5% (w/w). Reactions were set up in a 200µL final volume

containing 8μM pre-cleared actin and aldolase at the molar ratios specified in each experiment. Polymerisation was induced by addition of 10xPIB to a final 1x concentration and monitored by the increase in pyrene-fluorescence. Measurements were made using a Perkin-Elmer 3000 fluorimeter and calculation of the polymerisation half-time and rate at half-time were carried out as described in (Doolittle *et al.*, 2013). Apparent viscosity of actin solutions was measured using falling ball viscometry (Maclean-Fletcher and Pollard, 1980). Each sample was measured in triplicate and two independent samples measured for each aldolase:actin ratio tested.

Plant transformation procedures

Agrobacterium-mediated transient transformation of *Nicotiana tabacum* and *Nicotiana benthamiana* leaves was carried out according to (Sparkes *et al.*, 2006). Transformed leaf sections were imaged 48-72hrs after leaf infiltration with Agrobacterium. For transient transformation of *Nicotiana benthamiana,* leaves were co-infiltrated with an Agrobacterium strain containing a P19-expressing binary vector to prevent silencing of the other transiently transformed constructs of interest. Stably transformed Arabidopsis lines were generated using single and double floral-dipping methods described in (Davis *et al.*, 2009). The GFP:Lifeact line expressed in the Col-0 background was donated by Professor Patrick Hussey (University of Durham). Seeds of dipped plants were grown on MS-sucrose plates and selected with 15μgmL^{-1} glufosinate ammonium for RFP constructs and 15μgmL^{-1} hygromycin-B for GFP based constructs. Doubly transformed plants were screened with one of the two herbicides and the presence of the additional construct was verified by CLSM.

Arabidopsis growth and guard cell assays

Stomatal density measurements were carried out as described in (Jiang *et al.*, 2012). Plants were grown in a 'Microclima' growth chamber (Snijders Scientific) with a 22°C/20°C day/night temperature cycle and a 9.5/13.5hrs light/dark cycle separated by two 15min periods of intermediate light intensity and temperature, corresponding to dawn and dusk, for 5-6 weeks. Five-week-old plants were placed on a plastic horticultural tray and viewed under a thermal

imaging camera (model SC1000; FLIR Systems, Wilsonville, OR, USA). Thermal images were recorded at 1-min intervals. Leaf temperature was calculated as the average temperature of three different leaves on each of at least three different plants per genotype and plotted over time. For humidity-drop experiments, plants were monitored under daytime growing conditions (see above) for 50min, followed by a pre-programmed drop in the growth chamber's relative humidity from 80% to 40%. The experiments were repeated at least three times independently.

For growth analysis of Arabidopsis, wild type and mutant plants were germinated and grown for 10-12 days before transfer to soil and growth under normal conditions. Plants were imaged every 2 days, starting 2 days after transplanting and until plants bolted. Images were analysed using LeafLab version 4 software (Professor Mark Fricker, University of Oxford) to calculate total rosette leaf area.

Confocal laser-scanning microscopy and FRET-FLIM measurements

Confocal laser-scanning microscopy (CLSM) was carried out on a Zeiss (Jena, Germany) Axioplan 2 microscope with a water-dipping, 40x, 1.40NA objective lens, connected to an LSM510 Meta confocal module, or on a Leica (Solms, Germany) TCS-SP5 confocal microscope with a water-dipping, 63x, 1.20NA objective lens and appropriate settings for the various fluorophores. For imaging, plant samples were mounted in half-strength MS medium, 1% (w/v) sucrose, 0.05% (w/v) MES pH5.8 with KOH. For imaging guard cells, 4-6 week old rosette leaves were mounted in 10/50 buffer (10mM KCl, 50mM MES-KOH pH 6.15).

Co-localization analysis and calculation of the various coefficients was carried out using the JaCoP plugin in the Image J software (Bolte and Cordelieres, 2006). The local Pearson's correlation coefficient was estimated on a pixel-by-pixel basis from the structural term of the Structural Similarity Index (SSIM) (Zhou *et al.*, 2004) over an 2-D isotropic Gaussian-weighted region with radius of 5 pixels for each plane of dual-channel 3D (*x,y,z*) images of aldolase-RFP/LifeAct-GFP,

free-RFP/LifeAct-GFP, or aldolase-RGP/free-GFP. The resultant map of correlation coefficients was pseudo-colour coded between blue (-1, perfectly inversely-correlated) to red (1, perfectly correlated). For quantitative measurements, values were integrated over an elliptical binary region-of-interest (ROI) manually drawn to select a guard cell pair (excluding the nuclei), and further masked by an automatic intensity threshold from either the aldolase-RFP image or the LifeAct-GFP image to exclude background regions.

FRET-FLIM data was collected using a Leica SP5 confocal microscope connected to a PicoQuant (Berlin, Germany) PicoHarp 300, TCSPC (time-correlated single photon counting) FLIM module. FLIM images of GFP:Lifeact were acquired using a 470nm, pulsed laser for excitation and detector set to collect fluorescence between 500-560nm. 256x256 pixel images were collected until 1000 counts were achieved for each pixel. Post-acquisition analysis was carried out using the SymPhoTime 64 software from PicoQuant. The lifetimes of all the images per fluorophore combination were averaged and compared for the guard cells excluding the auto-fluorescence for the pore lips.

Results:

Plant aldolase interacts with actin *in vitro*

To determine whether plant aldolase interacts with actin and the impact on the functional properties of the two proteins, *in vitro* tests were conducted with purified recombinant *At*FBA8 (4.4mg total yield, 0.66 U mg^{-1} as assayed on the day of purification, and >90% pure as estimated by Coomassie stained gel, Supplementary Table S2, Supplementary Fig. S1) and actin. *At*FBA8 co-sedimented with polymerised F-actin, but not G-actin, in a concentration dependent manner. Thus, using SDS-PAGE and Coomassie blue staining, aldolase was detected in the supernatant fractions of G-actin and aldolase-only co-sedimentation samples, but the majority of aldolase was detected in the pellet fraction of the F-actin sample, with only traces being detectable in the corresponding supernatant (Fig. 1A, dashed arrow). In a similar co-sedimentation experiment increasing amounts of aldolase were added to a fixed

amount of actin (Fig. 1B) and aldolase was quantified by immuno-detection. At aldolase to actin monomer molar ratios of 0.3 or lower the majority of aldolase was associated with actin. Whereas, at molar ratios of 0.6 and above, the amount of aldolase co-pelleting with actin appeared to be saturated and additional aldolase accumulated in the supernatant.

The effects of aldolase binding on actin bundling and polymerisation were also investigated. Addition of aldolase at a molar ratio of 0.1 to F-actin led to a significant increase in viscosity compared to F-actin alone when measured by falling-ball viscometry (Fig. 2A). Further addition of aldolase at higher molar ratios to actin decreased viscosity to levels comparable to that of F-actin alone, as has been reported and explained for other actin bundling proteins (Wang *et al.*, 1996). Moreover, in a serial co-sedimentation experiment, aldolase co-pelleted both with bundled and unbundled F-actin (F-actin, Fig. 2B) but remained in the supernatant along with the majority of actin in the un-polymerised control sample (G-actin, Fig. 2B). However, addition of aldolase had no effect on actin polymerisation kinetics in pyrene fluorescence assays (Supplementary Fig. S2 and S3).

Reciprocally, aldolase enzyme activity assays showed that aldolase activity was significantly inhibited (3-fold decrease) in the presence of F-actin, but not G-actin or equimolar amounts of BSA. This was the case at both 5μM fructose 1,6-bisphosphate (F1,6-BP), which is close to the previously reported plant cytosolic aldolase K_M of 6μM (Moorhead and Plaxton, 1990), and at a saturating concentration of 5mM F1,6-BP (Fig. 2C). Aldolase activity was further measured in the presence of increasing amounts of F-actin (0-100μgmL^{-1}), corresponding to a decrease in the aldolase to actin molar ratio from 1.4 to 0.07) at a range of F1,6-BP concentrations (0-60μM). Michaelis-Menten curves were fitted to the resulting data (Fig. 2D) and the kinetic parameters of aldolase at each concentration of F-actin were calculated from these curves (Table 1). The inhibitory effect of actin was concentration dependent. At F-actin concentrations of 0-10μgmL^{-1} (molar ratio of aldolase to actin: infinity-0.7) there was a slight but progressive decrease in the aldolase V_{max} with the K_M remaining stable.

Aldolase activity further decreased by two orders of magnitude and then became undetectable at 50 and 100μgmL^{-1} F-actin (molar ratios of 0.14 and 0.07), respectively (Fig. 2D and Table 1). We infer from these data that plant aldolase can interact with F-actin *in vitro*, and the binding interaction has the potential to affect both the enzymatic activity of aldolase and the structure of the F-actin network.

Assessing association of aldolase with F-actin *in vivo.*

To determine whether aldolase FBA8 interacts with actin *in vivo*, we first sought to construct a fluorescently-tagged version of FBA8 that would functionally complement an FBA8-knockout Arabidopsis line (*fba8-1*). The *FBA8* coding sequence driven by the Arabidopsis ubiquitin-10 promoter was fused C-terminally with that of red fluorescent protein RFP (mRFP1). Expression of the full-length fusion protein was verified by western blot with an anti-aldolase antibody (Fig. 3A, solid arrow). Native aldolase was detectable in the wild type control at 40kD molecular weight, but not in the *fba8-1* genetic background of the transformants (Fig. 3A, dashed arrow). Intact aldolase:RFP in the complemented lines appeared at the expected 70kD (Fig. 3A, solid arrow), along with a cleavage product of the expected Mw of native aldolase. We assume that the partner cleavage product yielding free RFP might also be present in these lines, although we have not tested for its presence directly. Overall, FBA8-RFP protein level in the complemented lines was similar to wild type aldolase abundance. The complemented lines restored normal levels of germination and growth to the *fba8-1* mutant (Supplementary Fig. S4 and S5).

The subcellular localization of aldolase:RFP was compared to that of free RFP *in planta* using confocal laser-scanning microscopy (CLSM). Both aldolase:RFP and free RFP localized to the cytosol and the majority of fluorescence was homogeneously distributed, with smaller organelles (such as mitochondria) appearing in negative contrast. Free RFP (Mr 30kD) was able to enter the nucleus, whilst aldolase:RFP (Mr 70kD) was excluded as expected from the molecular weight cutoff size for protein import into the nucleus. Other than

this, no major difference in the distribution of the two fluorescent proteins was evident in root epidermal (Fig. 3B), hypocotyl cells (Fig. 3C), and in most other cell types studied, including: root meristem, root vascular and leaf epidermal cells (data not shown). However, in stomatal guard cells and to a lesser extent in leaf epidermal cells, a small proportion of aldolase:RFP was observed in association with fine filaments (Fig. 4A). In these cell types, aldolase:RFP was again excluded from chloroplasts and nuclei, but some signal was detectable in vacuoles that might reflect degradation of the aldolase:RFP observed in the western blots (Fig. 3A).

To test whether filamentous structures formed by aldolase:RFP represent instances of aldolase associating with actin, complemented *fba8-1* plants expressing aldolase:RFP, or Col-O plants expressing free RFP (as a control for a cytosolic protein not expected to associate with actin), were co-transformed with GFP:Lifeact, which binds to actin filaments (Riedl *et al.*, 2008). As an additional control for cytosolic protein colocalisation, complemented *fba8-1* plants expressing aldolase:RFP were also co-transformed with free cytosolic GFP. As expected, GFP:Lifeact labeled bundles and filaments of various thickness throughout the cytoplasm of guard cells and leaf epidermal cells (Fig. 4A and B), whilst free GFP was found throughout the cytosol, including cytoplasmic strands across the vacuole, and also within the nuclei (Fig. 4C). Merged images suggested some degree of co-localization between aldolase:RFP and GFP:Lifeact (Fig. 4A), but the degree of overlap was comparable to that seen in free RFP/GFP-lifeact images (Fig. 4B). Quantitative measurements of co-localisation using a suite of metrics including Pearson's correlation coefficient (PCC) and Manders overlap coefficients indicated some degree of co-localisation between aldolase:RFP and GFP:lifeact, but it was not significantly higher than that observed for free RFP and GFP:lifeact (Table 2). Conversely, there was a very high degree of visual overlap and correlation coefficient between free GFP and aldolase-RFP, except for the nuclei, where the latter is excluded. Van Steensel's cross correlation functions, Li's intensity correlation analysis, and Coste's analysis (Bolte and Cordelieres, 2006) were also carried out on the same images and also revealed no differences between aldolase:RPF and free RFP association

452 with GFP:Lifeact (Supplementary Table S3). Given that these correlation metrics
453 are averaged over the entire image, we further investigated spatially localized
454 estimates of PCC calculated as part of a Structural Similarity Index (SSIM)
455 measure (Zhou *et al.* 2004). However, pseudo-colour coded maps of the PCC
456 calculated for circular, Gaussian weighted regions around each pixel did not
457 provide evidence for higher co-localisation of aldolase:RFP along GFP:Lifeact
458 filaments (Fig. 4A-C). Taken together, we were not able to find quantitative
459 evidence for *in vivo* interaction between aldolase and actin using co-localisation
460 analysis. This finding is perhaps not surprising considering that only a small
461 fraction of total cellular aldolase may be bound to actin against a much more
462 substantial background of unbound, cytosolic aldolase, and confocal imaging
463 does not have sufficient spatial resolution to discriminate bound from free
464 aldolase.
465
466 We therefore sought a more specific test of interaction between
467 aldolase:RFP and GFP:Lifeact *in vivo* using fluorescence resonance energy
468 transfer-fluorescence lifetime imaging microscopy (FRET-FLIM). Measuring the
469 change of lifetime, if any, in GFP:Lifeact-aldolase:RFP co-expressing cells has the
470 benefit of eliminating any background signal from unbound cytosolic
471 aldolase:RFP (or cleaved free RFP), since the GFP:Lifeact fluorescence lifetime is
472 only sensitive to actin-bound aldolase:RFP within a few nm. Representative GFP
473 lifetime images of Arabidopsis guard cells expressing GFP:Lifeact alone and co-
474 expressing aldolase:RFP are shown in Fig. 5A. The majority of the cytoplasmic
475 GFP:Lifeact signal was within 2.3-2.7 ns, whilst the autofluorescence from the
476 pore lip showed a much longer lifetime of around 10 ns (Fig. 5A). However, the
477 average lifetime fit to the exponential decay curves showed evidence for an
478 interaction between aldolase:RFP and GFP:Lifeact as a slight, but significant,
479 decrease in the average lifetime. Thus, the average lifetime of GFP:Lifeact alone
480 was around 2.43ns but decreased to 2.39 ns when co-expressed with
481 aldolase:RFP (Fig. 5B). Similar results were found in transiently transformed
482 tobacco leaf epidermal cells (Fig. 5C). GFP:Lifeact alone or when it was co-
483 expressed with free RFP had an average lifetime of 2.60ns and 2.55ns,

484 respectively. When co-expressed with aldolase:RFP it had a significantly lower
485 average lifetime of 2.43ns.
486
487 If aldolase does indeed interact *in vivo* with actin at low concentration, we
488 would predict from the *in vitro* data that it might serve to stabilize or bundle
489 actin filaments. We therefore examined whether loss of aldolase in the *fba8-1*
490 mutant perturbed actin cytoskeleton organisation. The structure of actin was
491 compared by CLSM in guard cells of *fba8-1* and wild type plants expressing the
492 actin-binding GFP:Lifeact to visualise actin filaments and cables *in vivo*. There
493 was no major difference in the structure of the actin network between the two
494 lines. However, GFP:Lifeact in the *fba8-1* line (Fig. 6A) was slightly more diffuse,
495 with fewer thick actin cables compared to wild type or aldolase:RFP
496 complemented cells (Fig. 6B and C).
497

498 **Assessing the importance of aldolase FBA8 for guard cell function.**

499 As the cellular phenotype of the *fba8-1* mutant is quite subtle and
500 challenging to quantify, we sought to assess the importance of aldolase FBA8 for
501 guard cell function by characterizing physiological responses in the *fba8-1*
502 aldolase knockout line (Fig. 7A and B). This line had greatly decreased cytosolic
503 aldolase protein levels as verified by western blot with an anti-cytosolic aldolase
504 antibody (Fig. 7C) and significantly decreased aldolase enzyme activity in roots
505 (Fig. 7D) as measured by aldolase activity assays in crude protein extracts. It also
506 displayed moderately slow growth phenotypes, with *fba8-1* seedlings
507 germinated on MS agar plates without sucrose being smaller than wild type Col-
508 0 at one week old (Supplementary Fig. S4A). Additionally, rosettes of *fba8-1*
509 plants grown on sucrose supplemented MS agar plates and then transferred to
510 soil at two weeks old were smaller by 3 weeks old (Supplementary Fig. S4B and
511 C). This apparent difference in size was further confirmed by measuring rosette
512 leaf area of 24 individual plants per genotype (Supplementary Fig. S4D).
513

514 To assess guard cell function in the *fba8-1* and complemented
515 aldolase:RFP lines we used thermal imaging measurements of leaf temperature

as a proxy for transpiration over 24h day-night cycles. No differences in response were observed during dawn or dusk transitions (low light with increasing or decreasing temperature, respectively), or day (high light, 22°C) or night (dark, 20°C) conditions (Supplementary Fig. S6). However, during transition from high (80%) to low (40%) relative humidity (RH) the leaf temperature of *fba8-1* rosettes dropped to a greater extent than that of wild type or the complemented aldolase:RFP lines indicating greater stomatal aperture than wild type (Fig. 8). Thus, all three genotypes had similar temperatures under normal humidity conditions (Fig. 8, note overlapping traces in the left portion of the graph). However, upon reduction of humidity (dashed line) *fba8-1* leaves dropped to around 0.5°C cooler than those of Col-0 and aldolase:RFP over an extended period implying that *fba8-1* stomata reached a different set point in response to a change in RH. Moreover, this result was not caused by a difference in the density of stomata in *fba8-1* leaves (Supplementary Fig. S7).

Discussion

The data we have presented demonstrate that Arabidopsis aldolase FBA8 is capable of binding F-actin *in vitro* in a similar manner to aldolase from other organisms (Arnold and Pette, 1970; Wang *et al.*, 1996; Holtgrawe *et al.*, 2005). Moreover, this interaction affected the function of both these proteins. The effect of recombinant aldolase on F-actin viscosity we observed is most likely related to the presence of two putative actin-binding domains (Forlemu *et al.*, 2007) in the tetrameric aldolase holoenzyme (Moorhead and Plaxton, 1990) enabling it to bind two actin filaments simultaneously (Supplementary Fig. S8) and thereby act as an actin bundling protein. Indeed, addition of recombinant FBA8 to F-actin solutions and measurement of the concurrent change in viscosity generated a profile almost identical to that previously reported for rabbit muscle aldolase (Wang *et al.*, 1996) and similar to that expected for actin bundling proteins in general (Gungabissoon *et al.*, 2001). Wojtera-Kwiczor et al. (2012) previously proposed that FBA6, a different cytosolic isozyme of Arabidopsis aldolase, bundled actin under oxidizing but not under reducing conditions based on their results of actin phaloidin-staining followed by CLSM imaging. It was suggested

548 that such bundling of actin by aldolase under oxidising conditions may be part of
549 a greater signaling cascade occurring in response to changes in cellular redox
550 conditions. Thus, aldolase may have a secondary role as an actin bundling
551 protein.
552
553 In addition, we have shown that binding of aldolase to actin has reciprocal
554 effects on aldolase enzyme activity, resulting in non-competitive inhibition by F-
555 actin but not by equal amounts of G-actin or BSA. This effect is most likely due to
556 steric hindrance of the active site cleft upon binding actin filaments. It is also
557 interesting to note that uninhibited specific enzyme activity of *At*FBA8 we
558 purified from *Pichia pastoris* media is an order of magnitude lower than that of
559 native aldolases purified from carrot root (Moorhead and Plaxton, 1990) and
560 castor oil seeds (Moorhead *et al.*, 1994), but is comparable to that purified from
561 maize leaves (Gasperini and Pupillo, 1983).
562
563 To understand whether these quite strong reciprocal interactions
564 observed *in vitro* have any significance *in vivo* we sought to demonstrate first
565 that aldolase interacts with actin *in vivo*; second, whether this interaction affects
566 actin organization; and third, whether there is an effect on guard cell physiology
567 as a consequence. However, as any aldolase-actin interaction takes place against
568 a much greater background of free cytoplasmic aldolase and is well below the
569 resolution of CLSM it was not possible to identify co-localisation of a small
570 fraction of the aldolase pool with actin using conventional co-localisation
571 analysis, even when using local correlation measures. Use of the ubiquitin rather
572 than the native aldolase promoter to drive aldolase:RFP expression may have
573 caused some overexpression artefacts in our CLSM datasets and further
574 hampered our efforts. However, we consider this unlikely. Aldolase:RFP fusion
575 protein levels are comparable to native cytosolic aldolase in wild type plants
576 (Fig.3A) and we have seen none of the hallmarks of protein overexpression for
577 aldolase:RFP, such as accumulation in the nucleus or endomembrane system, in
578 any of our CLSM images. Nevertheless, our data provide some support for
579 microcompartmentation of aldolase FBA8 in guard cells using FRET-FLIM
580 measurements of GFP:Lifeact when co-expressed either with aldolase:RFP as a

much more specific measure of protein proximity, in either Arabidopsis guard cells or tobacco leaf epidermal cells. Our results show that in both cell types GFP:Lifeact has a significantly shorter lifetime when co-expressed with aldolase:RFP than GFP:Lifeact on its own or when co-expressed with free RFP. This finding suggests strongly that aldolase:RFP remains in proximity with GFP:Lifeact long enough to cause a reduction in the latter's fluorescence emission life-time. The simplest explanation for this observed effect is that the two fluorophores are anchored within a FRET-compatible distance (<10nm) by associating with actin filaments. The shift in lifetime is still small, possibly because we would still only expect a small number of aldolase:RFP molecules to bind within the Förster radius of the GFP-Lifeact molecules in an appropriate configuration for FRET.

Given the *in vitro* actin bundling property of aldolase FBA8, a potential role for the enzyme in guard cells could be to modify the actin cytoskeleton and thus modulate guard cell behaviour. Extensive reorganisation of the guard cell actin network occurs during stomatal movements (Kim *et al.*, 1995; Jiang *et al.*, 2012), and actin reorganisation is a critical link in the model of ABA-induced guard cell behavior (Li *et al.*, 2006). Previous work suggested that the polymeric state of actin affects guard cell motions, ostensibly by modulating inward rectifying K^+-channel activity. Cytochalasin-D treatments (which induce actin depolymerisation) of *Vicia faba* and *Commelina communis* leaves enhanced light-induced stomatal opening, while actin filament stabilizing agents inhibit this process (Kim *et al.*, 1995; Hwang *et al.*, 1997). It was also recently reported that the plant-specific stomatal closure-related actin binding protein 1 (SCAB1) protein bundles actin *in vitro* and *in* vivo in Arabidopsis. Moreover plants lacking this protein were hypersensitive to drought and showed impaired stomatal movements in response to ABA, hydrogen peroxide, and $CaCl_2$ treatments (Zhao *et al.*, 2011). We observed no effect of aldolase on actin polymerisation kinetics (Supplementary Fig. S2 and S3), but we have confirmed aldolase actin bundling *in vitro* (Fig. 2A and B). We infer that this might alter organisation of the actin network, and visual assessment of the actin filament network in *fba8-1* knockout guard cells suggested a subtle decrease in actin cable thickness in *fba8-1* stomata

and with a more anisotropic (parallel to each other) orientation compared to the thicker radial distribution of actin cables in wild type guard cells (Fig. 6D). This subtle cellular phenotype was matched by a subtle change in physiological responses: stomatal function in *fba8-1* leaves was unaffected under normal growth conditions (Supplementary Fig. S5). However, we showed that the *fba8-1* knockout line has altered stomatal responses to humidity changes: in the absence of FBA8, stomatal closure in response to low humidity was slightly impaired (Fig. 8). Whether or not this phenotype is linked to aldolase actin-bundling in stomata in a manner similar to SCAB1 or the actin related protein 2/3 (ARP2/3) complex (Jiang *et al.*, 2012) merits further investigation. Our findings suggests that aldolase FBA8 is requisite at least for some aspects of guard cell motion.

It is not possible to discern from our data whether this change in guard cell function is related to the metabolic function of aldolase or to a secondary role as an actin bundling protein. Indeed, a metabolic effect is plausible, given previous studies on knockout Arabidopsis lines of the glycolytic enzyme phosphoglycerate mutase showed a similarly slow response to ABA-induced closure (Zhao and Assmann, 2011). Since stomatal response to low humidity is primarily ABA-mediated (Assmann *et al.*, 2000; Xie *et al.*, 2006; Bauer *et al.*, 2013), it is conceivable that the delay in stomatal closure we observed is caused by a general metabolic impairment in glycolytic enzyme-knockout stomata and not related to aldolase microcompartmentation directly. Aldolase is required for both glycolysis and gluconeogenesis. While glycolysis (and thus aldolase) is clearly implicated in supplying carbon for malate production during stomatal opening (Vavasseur and Raghavendra, 2005), roles for glycolysis and/or gluconeogenesis during stomatal closure are less obvious. Results of ^{14}C-malate feeding experiments suggest that malate, exported from the vacuole during stomatal closure, is decarboxylated and converted to starch via gluconeogenesis (Outlaw, 1982). It was suggested that this is the main metabolic fate of malate during stomatal closure (Schroeder *et al.*, 2001). However, it has also been argued that the rate of malate conversion to starch in closing stomata is 3 orders of magnitude slower than stomatal closure itself, and that key enzymes activities

necessary for malate-fueled gluconeogenesis (such as pyruvate-phosphate dikinase and posphoenolpyruvate carboxykinase) are absent or very low in guard cells. Thus malate export from guard cells was proposed as an alternative (Outlaw, 2003), although it may also be catabolized via the TCA cycle (Santelia and Lawson, 2016). Our data from the *fba8-1* line and prior results from phosphoglycerate mutase knockout lines (Zhao and Assmann, 2011) are both consistent with a role for glycolysis or gluconeogenesis during ABA-mediated stomatal closure.

Ultimately, to discriminate between the enzymatic and actin-binding roles of aldolase, it will be necessary to genetically uncouple these two activities *in vivo*. We made concerted attempts to do this by mutating residues in aldolase that are thought to be responsible for actin binding (Supplementary Fig. S8). Unfortunately, the rather large change in charge caused by replacement of multiple residues affected the stability or folding of the protein, as we were unable to successfully express this mutant aldolase in Arabidopsis, yeast, or *E. coli* (data not shown).

In summary, we show clearly that plant aldolase can be microcompartmented *in vitro* as observed previously for mammalian aldolase, but identifying the extent that this occurs *in vivo* and the significance has proved to be more challenging. Our experiments provide some evidence that suggest this interaction also takes place *in vivo* and has some functional relevance. Firstly, aldolase:RFP but not free RFP formed filamentous structures, in addition to the expected homogeneous cytoplasmic distribution, that were reminiscent of the cytoskeleton. These filamentous structures co-localized with GFP:lifeact and resulted in a small, but significant decrease in the lifetime of GFP:lifeact in FRET-FLIM experiments. This last line of evidence is crucial, as it demonstrates a clear difference in the behavior of aldolase:RFP compared to free RFP, which is a presumably 'unbound' cytosolic protein. The consequence of normal FBA8 binding was assessed in *fba8-1* mutant lines that showed both a subtle decrease in actin network structure and a reduced closing response to a humidity drop. Thus we provide preliminary evidence for possible roles of aldolase in

organization of the actin cytoskeleton in stomatal guard cells, thereby complementing previous findings, which suggest that Arabidopsis cytosolic aldolases moonlight as actin bundling proteins.

Supplementary Data

Supplementary Table S1: Primers and PCR annealing temperatures used;
Supplementary Table S2: Recombinant *At*FBA8 purification chart
Supplementary Table S3: Metrics of aldolase:RFP and free RFP co-localisation with GFP:Lifeact in Arabidopsis guard cells;
Supplementary Figure S1: Purification of AtFBA8 from *Pichia pastoris* media
Supplementary Figure S2: Pyrene fluorescence assay of actin polymerisation in the presence of recombinant aldolase;
Supplementary Figure S3: Kinetics of actin polymerisation in the presence of recombinant aldolase;
Supplementary Fig. S4: Germination and growth phenotypes of *fba8-1* aldolase-knockout line;
Supplementary Fig. S5: Complementation of *fba8-1* phenotypes by aldolase:RFP;
Supplementary Fig. S6: Thermal imaging data on *fba8-1* during a normal growth cycle;
Supplementary Fig. S7: Stomatal density and index of the *fba8-1* line;
Supplementary Fig. S8: Identification of putative actin-binding residues and sites of Arabidopsis FBA8;

Acknowledgements:

CG would like to thank Doctors: B. Ghel, A. Kugler, M. Laxa, N. Irani, M. Kalde and B. O'Leary (University of Oxford, UK) for their invaluable help and training in experimental techniques during this project. We thank Dr. M. Schwarzlander (University of Bonn, Germany) for the roGFP2 expression vector, Professor B. Davis and B. Bhushan (University of Oxford, UK) for help with expressing recombinant aldolase and Professor W. Plaxton (Queen's University, Ontario, Canada) for the anti-aldolase antibody. We also thank Dr. Ian Moore (University of Oxford, UK) for help and advice with CLSM experimental design.

CG and LJS acknowledge funding from the Gatsby Charitable foundation.

Declaration of Interest: The authors declare no conflicts of interest.

Contribution Statement: CG conducted experiments and wrote the paper; MDF conducted experiments, provided analytical software, and wrote the paper; KIK, TJH, and IC provided technical expertise, and helped design and conduct experiments; PJH and AMH helped design experiments and contributed materials for their completion; LJS conceived and designed experiments, and wrote the paper.

References:

An S, Deng YJ, Tomsho JW, Kyoung M, Benkovic SJ. 2010. Microtubule-assisted mechanism for functional metabolic macromolecular complex formation. *Proceedings of the National Academy of Sciences of the United States of America* **107**, 12872-12876.

An S, Kumar R, Sheets ED, Benkovic SJ. 2008. Reversible compartmentalization of de novo purine biosynthetic complexes in living cells. *Science* **320**, 103-106.

Arnold H, Pette D. 1970. Binding of aldolase and triosephosphate dehydrogenase to F-actin and modification of catalytic properties of aldolase. *European Journal of Biochemistry* **15**, 360-366.

Assmann SM, Snyder JA, Lee Y-rJ. 2000. ABA-deficient (*aba1*) and ABA-insensitive (*abi1-1, abi2-1*) mutants of Arabidopsis have a wild-type stomatal response to humidity. *Plant Cell and Environment* **23**, 387-395.

Atteia A, Adrait A, Brugiere S, Tardif M, van Lis R, Deusch O, Dagan T, Kuhn L, Gontero B, Martin W, Garin J, Joyard J, Rolland N. 2009. A proteomic survey of Chlamydomonas reinhardtii mitochondria sheds new light on the metabolic plasticity of the organelle and on the nature of the alpha-proteobacterial mitochondrial ancestor. *Molecular Biology and Evolution* **26**, 1533-1548.

Balasubramanian R, Karve A, Kandasamy M, Meagher RB, Moore BD. 2007. A role for F-Actin in hexokinase-mediated glucose signaling(1[C][W][OA]). *Plant Physiology* **145**, 1423-1434.

Barkla BJ, Vera-Estrella R, Hernandez-Coronado M, Pantoja O. 2009. Quantitative proteomics of the tonoplast reveals a role for glycolytic enzymes in salt tolerance. *The Plant Cell* **21**, 4044-4058.

Bauer H, Ache P, Lautner S, Fromm J, Hartung W, Al-Rasheid KA, Sonnewald S, Sonnewald U, Kneitz S, Lachmann N, Mendel RR, Bittner F, Hetherington AM, Hedrich R. 2013. The stomatal response to reduced relative humidity requires guard cell-autonomous ABA synthesis. *Current biology : CB* **23**, 53-57.

Bolte S, Cordelieres FP. 2006. A guided tour into subcellular colocalization analysis in light microscopy. *Journal of Microscopy-Oxford* **224**, 213-232.

Chuong SD, Good AG, Taylor GJ, Freeman MC, Moorhead GB, Muench DG. 2004. Large-scale identification of tubulin-binding proteins provides insight on subcellular trafficking, metabolic channeling, and signaling in plant cells. *Molecular Cell Proteomics* **3**, 970-983.

Davis AM, Hall A, Millar AJ, Darrah C, Davis SJ. 2009. Protocol: Streamlined sub-protocols for floral-dip transformation and selection of transformants in *Arabidopsis thaliana*. *Plant Methods* **5**.

Deeks MJ, Fendrych M, Smertenko A, Bell KS, Oparka K, Cvrckova F, Zarsky V, Hussey PJ. 2010. The plant formin AtFH4 interacts with both actin and microtubules, and contains a newly identified microtubule-binding domain. *Journal of Cell Science* **123**, 1209-1215.

Doolittle LK, Rosen MK, Padrick SB. 2013. Measurement and analysis of *in vitro* actin polymerization. *Methods in molecular biology* **1046**, 273-293.

Feric M, Vaidya N, Harmon TS, Mitrea DM, Zhu L, Richardson TM, Kriwacki RW, Pappu RV, Brangwynne CP. 2016. Coexisting liquid phases underlie nucleolar subcompartments. *Cell* **165**, 1686-1697.

Forlemu NY, Waingeh VF, Ouporov IV, Lowe SL, Thomasson KA. 2007. Theoretical study of interactions between muscle aldolase and F-actin: Insight into different species. *Biopolymers* **85**, 60-71.

Gasperini G, Pupillo P. 1983. Aldolase isozymes in maize leaves. *Plant Science Letters* **28**, 163-171.

Giege P, Heazelwood, Roessner-Tunali, Millar H, Fernie AR, Leaver CJ, Sweetlove LJ. 2003. Enzymes of glycolysis are functionally associated with the mitochondrion in Arabidopsis cells. *The Plant Cell* **15**, 2140-2151.
Gierasch LM, Gershenson A. 2009. Post-reductionist protein science, or putting Humpty Dumpty back together again. *Nature Chemical Biology* **5**, 774-777.
Graham JW, Williams TC, Morgan M, Fernie AR, Ratcliffe RG, Sweetlove LJ. 2007. Glycolytic enzymes associate dynamically with mitochondria in response to respiratory demand and support substrate channeling. *The Plant Cell* **19**, 3723-3738.
Graham JWA. 2007. Mitochondrial glycolysis in plants. *DPhil Thesis, University of Oxford*.
Grefen C, Donald N, Hashimoto K, Kudla J, Schumacher K, Blatt M, R. 2010. A ubiqutin-10 promoter-based vector set for fluorescent tagging facilitates temporal stability and native distrbution in transient and stable expression studies. *The Plant Journal* **64**, 355-365.
Guex N, Peitisch MC. 1997. SWISS-MODEL and the Swiss-PdbViewer: An environment for comparative protein modeling. *Electrophoresis* **18**, 2714-2723.
Gungabissoon RA, Khan S, Hussey PJ, Maciver SK. 2001. Interaction of elongation factor 1α from *Zea mays* (ZmEF-1α) with F-actin and interplay with the maize actin severing protein, ZmADF3. *Cell Motility and the Cytoskeleton* **49**, 104-111.
Holtgrawe D, Scholz A, Altmann B, Scheibe R. 2005. Cytoskeleton-associated, carbohydrate-metabolizing enzymes in maize identified by yeast two-hybrid screening. *Physiologia Plantarum* **125**, 141-156.
Hrazdina G, Wagner GJ. 1985. Metabolic pathways as enzyme complexes: Evidence for the synthesis of phenylpropanoids and flavonoids on membrane associated enzyme complexes. *Archives of Biochemistry and Biophysics* **237**, 88-100.
Hruz T, Laule O, Szabo G, Wessendorp F, Bleuler S, Oertle L, Widmayer P, Gruissem W, Zimmermann P. 2008. Genevestigator v3: a reference expression database for the meta-analysis of transcriptomes. *Advances in Bioinformatics* **2008**, 420747.
Huang S, Taylor NL, Narsai R, Eubel H, Whelan J, Millar AH. 2009. Experimental analysis of the rice mitochondrial proteome, its biogenesis, and heterogeneity. *Plant Physiology* **149**, 719-734.
Hudder A, Nathanson L, Deutscher MP. 2003. Organization of Mammalian Cytoplasm. *Molecular and Cellular Biology* **23**, 9318-9326.
Hwang J-U, Suh S, Yi H, Kim J, Lee Y. 1997. Actin filaments modulate both stomatal opening and inward rectifying K+-channel activities in guard cells of *Vicia faba* L. . *Plant Physiology* **115**, 335-342.
Jiang K, Sorefan K, Deeks MJ, Bevan M, Hussey PJ, Hetherington AM. 2012. The ARP2/3 complex mediates guard cell actin reorganization and stomatal movement in Arabidopsis. *The Plant Cell* **24**, 2031-2040.
Kim M, Hepler PK, Eun S-O, Ha KS, Lee Y. 1995. Actin filaments in mature guard cells are radially distributed and involved in stomatal movement. *Plant Physiology* **109**, 1077-1084.
Li S, Assmann SM, Albert R. 2006. Predicting essential components of signal transduction networks: A dynamic model of guard cell absicic acid signaling. *PLoS Biology* **4**, 1732-1748.
Maclean-Fletcher SD, Pollard TD. 1980. Viscometric analysis of the gelation of Acanthamoeba extracts and purification of 2 gelation factors. *Journal of Cell Biology* **85**, 414-428.
Moller BL. 2010. Dynamic Metabolons. *Science* **330**, 1328-1329.
Moorhead G, BG., Hodgson RJ, Plaxton WC. 1994. Copurification of cytosolic fructose 1,6-bisphosphatase and cytosolic aldolase from endosperm of germinating castor oil seeds. *Archives of Biochemistry and Biophysics* **312**, 326-335.
Moorhead G, BG., Plaxton WC. 1990. Purification and characterization of cytosolic aldoalse from carrot storage root. *Biochemical Journal* **269**, 133-139.

Olah J, Norris V, Ovadi J. 2015. Modeling of sensing potency of cytoskeletal systems decorated with metabolic enzymes. *Journal of Theoretical Biology* **365**, 190-196.
Outlaw WHJ. 1982. *Carbon metabolism in guard cells*. New York: Springer Science.
Outlaw WHJ. 2003. Integration of cellular and physiological functions of guard cells. *Critical Reviews in Plant Sciences* **22**, 503-529.
Riedl J, Crevenna AH, Kessenbrock K, Yu JH, Neukirchen D, Bista M, Bradke F, Jenne D, Holak TA, Werb Z, Sixt M, Wedlich-Soldner R. 2008. Lifeact: a versatile marker to visualize F-actin. *Nature Methods* **5**, 605-607.
Santelia D, Lawson T. 2016. Rethinking guard cell metabolism. *Plant Physiol* **172**.
Sayle R, Milner-White JE. 1995. RasMol: Biomolecular graphics for all. *Trends in Biochemical Sciences* **20**.
Schindelin J, Arganda-Carreras IE, Frise., Verena Kaynig ML, Tobias Pietzsch, Stephan Preibisch, Curtis Rueden, Stephan Saalfeld, Benjamin Schmid, Jean-Yves Tinevez, Daniel James White, Volker Hartenstein, Kevin Eliceiri, Pavel Tomancak and Albert Cardona. 2012. Fiji: an open-source platform for biological-image analysis. *Nature Methods* **9**, 676-682.
Schroeder JI, Allen GJ, Hugouvieux V, Kwak JM, Waner D. 2001. Guard cell signal transduction. *Annual Reviews in Plant Physiology and Plant Molecular Biology* **52**, 627-658.
Schwarzlander M, Fricker MD, Sweetlove LJ. 2009. Monitoring the in vivo redox state of plant mitochondria: effect of respiratory inhibitors, abiotic stress and assessment of recovery from oxidative challenge. *Biochimica Et Biophysica Acta* **1787**, 468-475.
Sparkes IA, Runions J, Kearns A, Hawes C. 2006. Rapid, transient expression of fluorescent fusion proteins in tobacco plants and generation of stably transformed plants. *Nature Protocols* **1**, 2019-2025.
Sullivan DTMR, Fuda N., Fiori J., Barilla J., Ramirez L. 2003. Analysis of glycolytic enzyme co-localization in Drosophila flight muscle. *The Journal of Experimental Biology* **206**, 2031-2038.
Sweetlove LJ, Fernie AR. 2013. The spatial organization of metabolism within the plant cell. *Annual Review of Plant Biology* **64**, 723-746.
Vavasseur A, Raghavendra AS. 2005. Guard cell metbolism and CO2 sensing. *New Phytologist* **165**, 665-682.
Wang J, Morris AJ, Tolan DR, Pagliaro Len. 1996. Molecular nature of the F-actin binding activity of aldolase revealed with site-directed mutants. *The Journal of Biological Chemistry* **271**, 6861-6865.
Wojtas K, Slepecky N, von Kalm L, Sullivan DT. 1997. Flight muscle function in *Drosophila* requires colocalization of glycolytic enzymes. *Molecular Biology of the Cell* **8**, 1665-1675.
Wojtera-Kwiczor J, Gross F, Leffers HM, Kang M, Schneider M, Scheibe R. 2012. Transfer of a redox-signal through the cytosol by redox-dependent microcompartmentation of glycolytic enzymes at mitochondria and actin cytoskeleton. *Frontiers in plant science* **3**, 284.
Xie X, Wang Y, Williamson L, Holroyd GH, Tagliavia C, Murchie E, Theobald J, Knight MR, Davies WJ, Leyser HM, Hetherington AM. 2006. The identification of genes involved in the stomatal response to reduced atmospheric relative humidity. *Current biology : CB* **16**, 882-887.
Zhao Y, Zhao S, Mao T, Qu X, Cao W, Zhang L, Zhang W, He L, Li S, Ren S, Zhao J, Zhu G, Huang S, Keqiong Y, Yuan M, Guo Y. 2011. The plant-specific acin binding protein SCAB1 stabilizes actin filaments and regulates stomatal movement in Arabidopsis. *The Plant Cell* **23**, 2314-2330.
Zhao Z, Assmann SM. 2011. The glycolytic enzyme, phosphoglycerate mutase, has critical roles in stomatal movement, vegetative growth, and pollen production in Arabidopsis thaliana. *Journal of Experimental Botany* **62**, 5179-5189.

Zhou W, Bovik AC, Sheikh HR, Simoncelli EP. 2004. Image quality assessment: from error visibility to structural similarity. *IEEE Transactions on Image Processing* **13**, 600-612.

Tables, Figure legends, Figures

Table 1: Kinetic parameters of recombinant aldolase FBA8 in the presence of F-actin. V

	[Actin] µgmL^{-1} (aldolase to actin monomer molar ratio)				
Aldolase kinetic parameter	**0 (*)**	**5 (1.4)**	**10 (0.7)**	**50 (0.14)**	**100 (0.07)**
K_M for F1,6-BP (µM)	3.6±1.0	5.4±0.8	5.4±1.1	*	*
V_{max} (U mg^{-1})	0.054±0.003	0.046±0.003	0.042±0.002	0.001	0
Correlation coefficient[1]	0.98	0.88	0.87	*	*
Residuals[2]	8.7*10^{-5}	5*10^{-4}	4*10^{-4}	1.9*10^{-5}	*

Values shown are the average±S.E.M. of three technical replicates. V_{max} values for all samples in the presence of F-actin were significantly lower than the uninhibited control (0) at P<0.05 using Students two-tailed homoscedastic t-test. K_M were not significantly different.

* not applicable

[1]Pearson's correlation coefficient between experimental and calculated velocity data shown in Figure 2C

[2]Minimum sum of squares used to find best fitting Michaelis Menten curve to experimental data shown in Figure 2C

Table 2: Co-localisation parameters of aldolase:RFP with GFP:Lifeact or free GFP, and of free RFP with GFP:Lifeact

Co-localisation coefficient*:	GFP:Lifeact/ aldolase:RFP	GFP:Lifeac/ free RFP	Free GFP/ Aldolase:RFP
Pearson's	0.50±0.01	0.52±0.02	0.73±0.01
Overlap	0.80±0.01	0.80±0.02	0.85±0.01
Manders M1 (GFP:Lifeact)	0.47±0.05	0.57±0.06	0.81±0.07
Manders M2 (aldolase:RFP/free RFP)	0.38±0.03	0.42±0.05	0.69±0.04

* Values are the average of each co-efficient ± S.E.M. calculated from a minimum of six independent CLSM, z-stack image series (*n*=6), for each of the individual co-expressing lines.

** **Figure 1: Association of aldolase with actin *in vitro*.** A) An actin co-sedimentation assay using recombinant Arabidopsis aldolase (0.05mgmL^{-1}, monomer molar ratio to actin of ~0.1). Reagents added to each sample are shown in the table above the gel image. Actin samples (0.5mgmL^{-1}) were allowed to polymerise in a final volume of 1mL, centrifuged to precipitate F-actin, and the resulting pellet (P) and supernatant (S) fractions analysed by SDS-PAGE followed by Coomassie staining. Actin bands, indicated by solid arrow, are present in all lanes due to carry-over during sample loading. Aldolase bands are indicated by a dashed arrow. The protein concentration of each fraction prior to loading is show below the corresponding lane B) Supernatant and pellet fractions of a co-sedimentation assay similar to that shown in A. A fixed amount of actin (0.5mg mL^{-1}) was polymerised in the presence of increasing molar ratios of aldolase (shown above each lane, 0.05-0.5mgmL^{-1}) and samples of 0.5mL final volume were centrifuged. Resulting fractions were analysed by SDS-PAGE and western blotting with an anti-aldolase primary antibody, comparable amounts of each fraction were loaded per lane. Aldolase-actin molar ratios are shown above the fractions from each sample. Approximate molecular weight is shown on the right of each gel or blot. Supernatant and pellet fractions derived from the same sample are vertically aligned. Values below each lane are relative quantities (estimated by densitometry) as a percent of total protein detected in both corresponding pellet and supernatant fractions.

**** Figure 2: Aldolase actin binding has reciprocal functional effects *in vitro*.** A) Falling-ball viscosity measurements of G- and F-actin samples in the presence of increasing molar ratios of aldolase. Numbers in () indicate the molar ratio of aldolase to actin monomers in each sample. (a) Denotes a significant difference compared to G-actin and (b) compared to F-actin (0) samples at $P<0.01$ using Student's, two-tailed, homoscedastic t-test. B) Serial co-sedimentation assays set up as in Fig. 1B. After polymerization samples were centrifuged at low speed, the supernatant from this step was then centrifuged at high speed and the resulting fractions analysed by SDS-PAGE and Coomassie staining. Equal volumes were run in each lane. G-actin: un-polymerised actin control with aldolase, F-actin: polymerized actin with aldolase, B: low-speed "bundled actin" pellet fraction, P:

high-speed pellet fraction, S: supernatant after high-speed centrifugation. Actin (solid arrow) and aldolase (dashed arrow) and approximate molecular weights are indicated. Values below each lane are the relative amounts of actin and aldolase estimated from the image, normalized to G-actin supernatant band intensity; C) Aldolase specific activity in the presence of F-actin, G-actin, and BSA, at molar ratios of ~0.1 aldolase to other proteins and at two different concentrations of fructose-1,6 bisphosphate. (a) denotes a significant difference compared to corresponding G-actin sample and (b) to corresponding BSA sample at $P<0.01$ using Student's, two-tailed, homoscedastic t-test. D) Michaelis-Menten curves of aldolase activity in the presence of increasing amounts of polymerised actin. All values are the average of at least three technical replicates. Error bars are S.E.M. Experiments were repeated at least twice with reproducible results.

**** Figure 3: Distribution of aldolase:RFP and free RFP expressed in an Arabidopsis aldolase knockout genetic background in seedling root epidermal and hypocotyl cells imaged by CLSM.** A) Western blot on crude protein extracts from wild type (Col-0), aldolase knockout (*fba8-1*), and three independent aldolase:RFP expressing plants (ARFP1, 2, and 3) from leaves of 5 week-old plants using an anti-aldolase primary antibody. Approximate molecular weights of 70kD and 40 kD (arrows) as estimated by comparison to a molecular weight marker are indicated. The Ponceau S stained membrane before probing with the anti-aldolase antibody is shown as a loading control. Approximately 40µg protein was loaded per lane; B) Free RFP and aldolase:RFP in root epidermal cells; C) Free RFP and aldolase:RFP in hypocotyl cells; Seedlings used for imaging were 10-14 days old.

** **Figure 4: Investigating the correlation of aldolase:RFP and free RFP with GFP:Lifeact, and aldolase:RFP with free GFP in Arabidopsis *fba8-1* guard cells using CLSM.** Maximal intensity z-series projections of guard cells co-expressing: A) GFP:Lifeact with aldolase:RFP; B) GFP:Lifeact with free RFP; and C) free, cytosolic GFP with aldolase:RFP; GFP fluorescence (GFP:Lifeact and free GFP) is pseudocoloured green, RFP fluorescence (aldolase:RFP and free RFP) is

pseudocoloured magenta, co-localizing voxels in the merged images are shown in white. The PCC panel is a pseudocoloured image showing the Pearson's correlation coefficient of the co-expressed fluorophores in each pixel, with blue indicating low correlation and red indicating maximum correlation of the two fluorophores (see reference bar below images), p: plastid, sp: stomatal pore, n: nucleus, v: vacuole; D) Spatially averaged Pearson's correlation coefficient (PCC) of GFP:Lifeact with aldolase:RFP (GFPLA/ARFP) or with free RFP (GFPLA/RFP), and free GFP with aldolase:RFP (freeGFP/ARFP). Values are the spatially averaged co-efficient ± S.E.M calculated from a minimum of seven independent CLSM, z-stack image series (n=7) for each of the co-expressing lines.

** **Figure 5: FRET-FLIM measurements of GFP:Lifeact expressed in Arabidopsis guard cells and in tobacco leaf epidermal cells.** A) GFP:Lifeact expressed alone (GFP:Lifeact) and co-expressed with aldolase:RFP (GFP:Lifeact/ARFP) in Arabidopsis *fba8-1* guard cells. Images are color-coded according to the lifetime (in ns) of GFP in each pixel, a reference bar with the range of lifetimes is shown below the images. B) Average lifetime of GFP:Lifeact when expressed alone (GFPLA), or co-expressed with aldolase:RFP (ARFP/GFPLA) in Arabidopsis *fba8-1* guard cells. C) Average lifetime of GFP:Lifeact expressed alone (GFPLA), co-expressed with aldolase:RFP (ARFP/GFPLA), or with free RFP (RFP/GFPLA) in tobacco leaf epidermal cells. Values are the average lifetime of nine independent images per line for both Arabidopsis and tobacco experiments, error bars are S.E.M. Three different images were taken from each of three leaves originating from different plants (n=9). Average lifetimes for each image were calculated from regions of interest that excluded lifetime values from the stomatal pore region (arrowheads in A), where strong auto-fluorescence would result in spuriously high lifetime values. (a) is significantly different from corresponding GFPLA and (b) is significantly different from the RFP/GFPLA at P<0.01 using Student's, two-tailed, homoscedastic t-test.

** **Figure 6: Distribution of actin in guard cells of *fba8-1*, aldolase:RFP complemented and wild type plants.** GFP:Lifeact expressed in: A) *fba8-1,* B)

aldolase:RFP complemented, and C) wild type Col-0 Arabidopsis guard cells. Images are maximal intensity projections of z-stack confocal series. Comparable images were acquired from at least three different leaves per line, originating from different plants.

**** Figure 7: Schematic gene model of Arabidopsis aldolase *FBA8* (*At3g52930*) and isolation of an *FBA8* knockout line.** A) Schematic diagram of the *FBA8* gene. 5'- (box) and 3'- (box arrow) un-translated regions (UTRs) are shown in light grey. Exons are shown as dark grey boxes. Introns are shown as lines. The approximate insertion sites of the T-DNA insertions in lines *fba8-1* (used in this work), *fba8-2,* and *fba8-3*, are indicated with white arrowheads. B) Shows the results of an RT-PCR targeting the full-length mature transcript of the aldolase gene and of an RT-PCR on the same cDNA, but targeting a fragment of a ubiquitin transcript as a reference, in individual *fba8-1* plants, progeny of a segregating plant population. Numbers 1, 2, 3, and 4 denote individual heterozygous (1 and 2) and homozygous (3 and 4) plants. C) Is a western blot with an anti-cytosolic aldolase antibody on crude protein extracts from wild type Col-0 and homozygous *fba8-1* leaves. Mw or aldolase band (arrow) is between 35-40kD D) Crude protein extracts from roots and leaves of wild type and *fba8-1* homozygous seedlings were assayed for total aldolase enzyme activity. Values are the average of two technical replicates from at least two biological samples (>20 seedlings per replicate) for each genotype. Error bars are S.E.M. * is significantly different from the corresponding Col-0 sample at $P<0.01$ using Student's, two tailed, homoscedastic t-test. The experiment was repeated twice with similar results.

****Figure 8: Leaf temperature of *fba8-1* during a humidity drop treatment.**
A) Leaf temperature was measured by infrared imaging. Plants were imaged at 80% relative humidity (RH) for fifty minutes. Humidity was decreased to 40% RH and plants were imaged for over two hours. The dashed line indicates the time point where humidity began to decrease. Leaf temperature was compared to Col-0 and aldolase:RFP expressing *fba8-1* plants. Ambient temperature was measured in parallel. Values are the average temperature of three different

leaves from three different plants (*n*=9) per line, error bars are S.E.M. *Fba8-1* leaf temperature was found to be significantly different from Col-0 and aldolase:RFP after the drop in RH, using one-way ANOVA.

A

Reagent	Sample					
	F-actin		Aldolase		G-actin	
	P	S	P	S	P	S
Actin	+	+	-	-	+	+
Aldolase	+	+	+	+	+	+
Polymerisation buffer	+	+	+	+	-	-

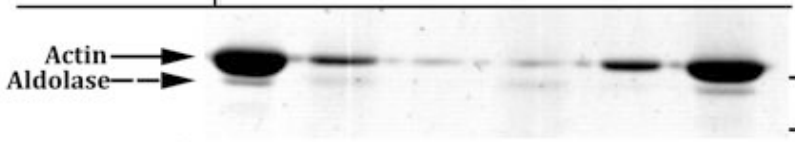

Protein mgmL^{-1}	1.1	0.3	0.0	0.1	0.2	0.6

B

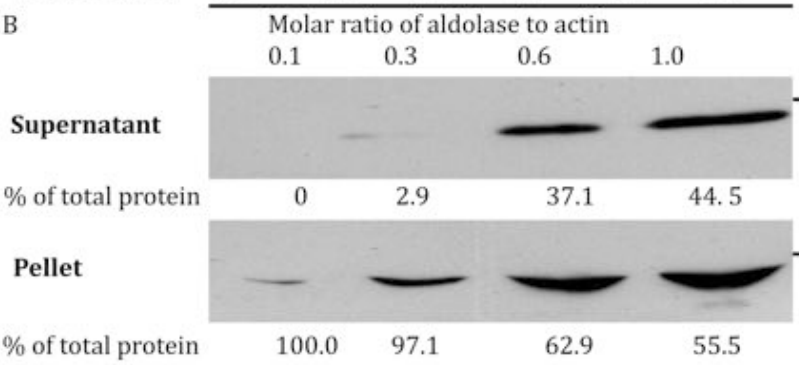

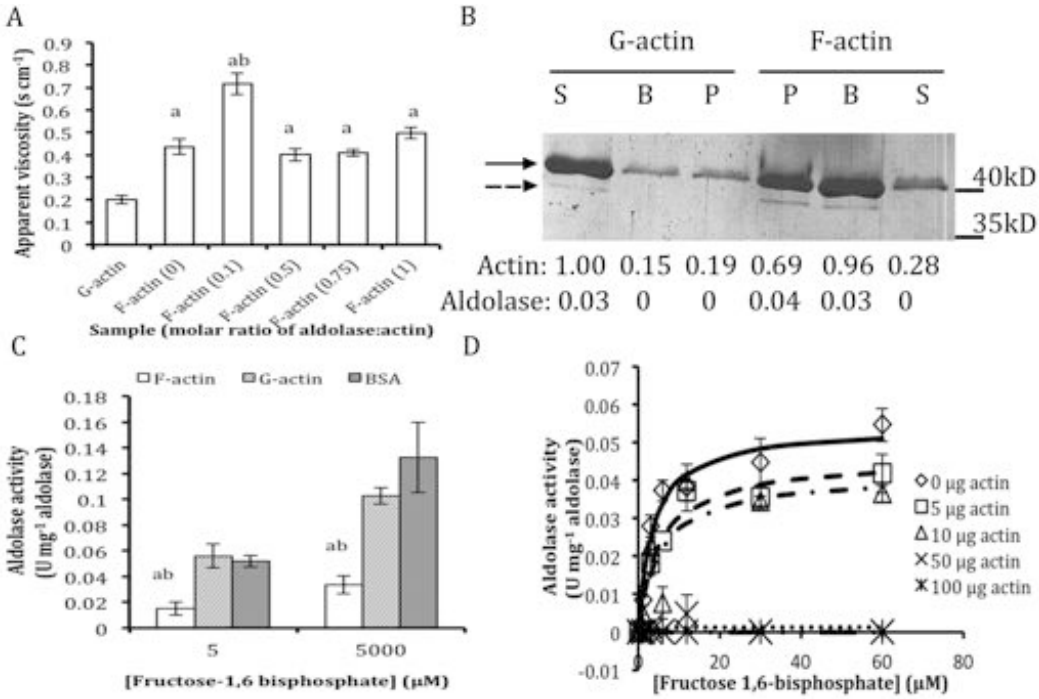
A
Apparent viscosity (s cm⁻¹)
0.9
0.8
0.7
0.6
0.5
0.4
0.3
0.2
0.1
0
a
ab
a
a
a
G-actin
F-actin (0)
F-actin (0.1)
F-actin (0.5)
F-actin (0.75)
F-actin (1)
Sample (molar ratio of aldolase:actin)
B
G-actin
F-actin
S
B
P
P
B
S
40kD
35kD
Actin: 1.00 0.15 0.19 0.69 0.96 0.28
Aldolase: 0.03 0 0 0.04 0.03 0
C
F-actin
G-actin
BSA
Aldolase activity (U mg⁻¹ aldolase)
0.18
0.16
0.14
0.12
0.1
0.08
0.06
0.04
0.02
0
ab
ab
5
5000
[Fructose-1,6 bisphosphate] (μM)
D
Aldolase activity (U mg⁻¹ aldolase)
0.07
0.06
0.05
0.04
0.03
0.02
0.01
0
-0.01
0
20
40
60
80
[Fructose 1,6-bisphosphate] (μM)
0 μg actin
5 μg actin
10 μg actin
50 μg actin
100 μg actin

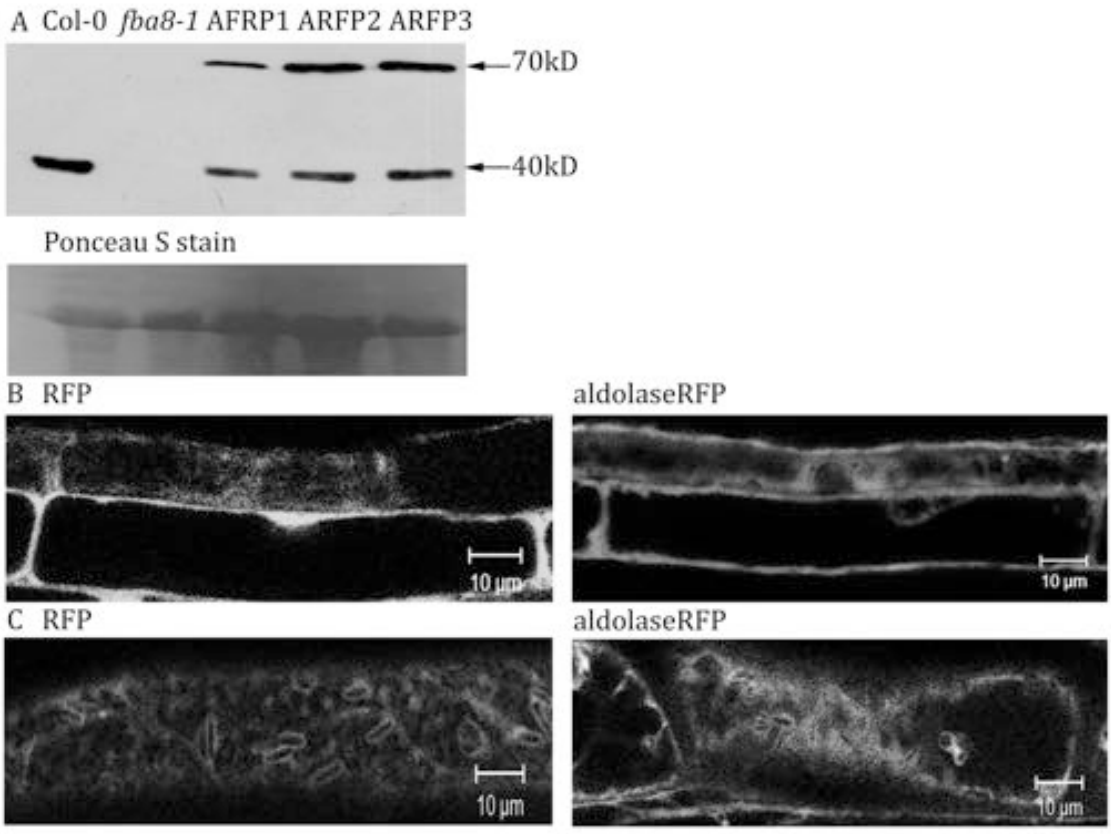
A Col-0 fba8-1 AFRP1 ARFP2 ARFP3
70kD
40kD
Ponceau S stain
B RFP
aldolaseRFP
10 μm
10 μm
C RFP
aldolaseRFP
10 μm
10 μm

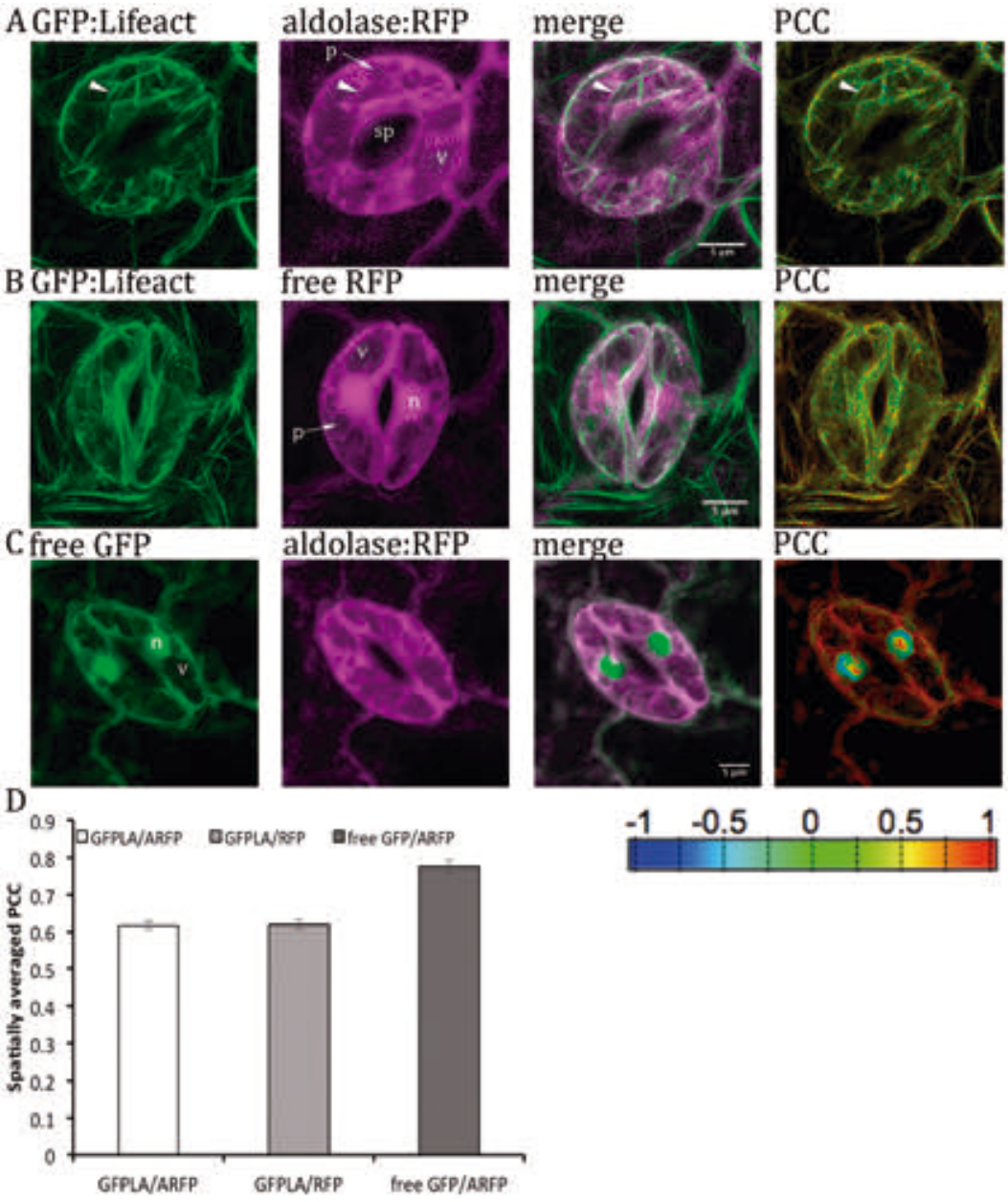
A GFP:Lifeact
aldolase:RFP
merge
PCC
p
sp
v
B GFP:Lifeact
free RFP
merge
PCC
v
n
p
C free GFP
aldolase:RFP
merge
PCC
n
v
D
-1
-0.5
0
0.5
1
GFPLA/ARFP
GFPLA/RFP
free GFP/ARFP
Spatially averaged PCC
0.9
0.8
0.7
0.6
0.5
0.4
0.3
0.2
0.1
0
GFPLA/ARFP
GFPLA/RFP
free GFP/ARFP

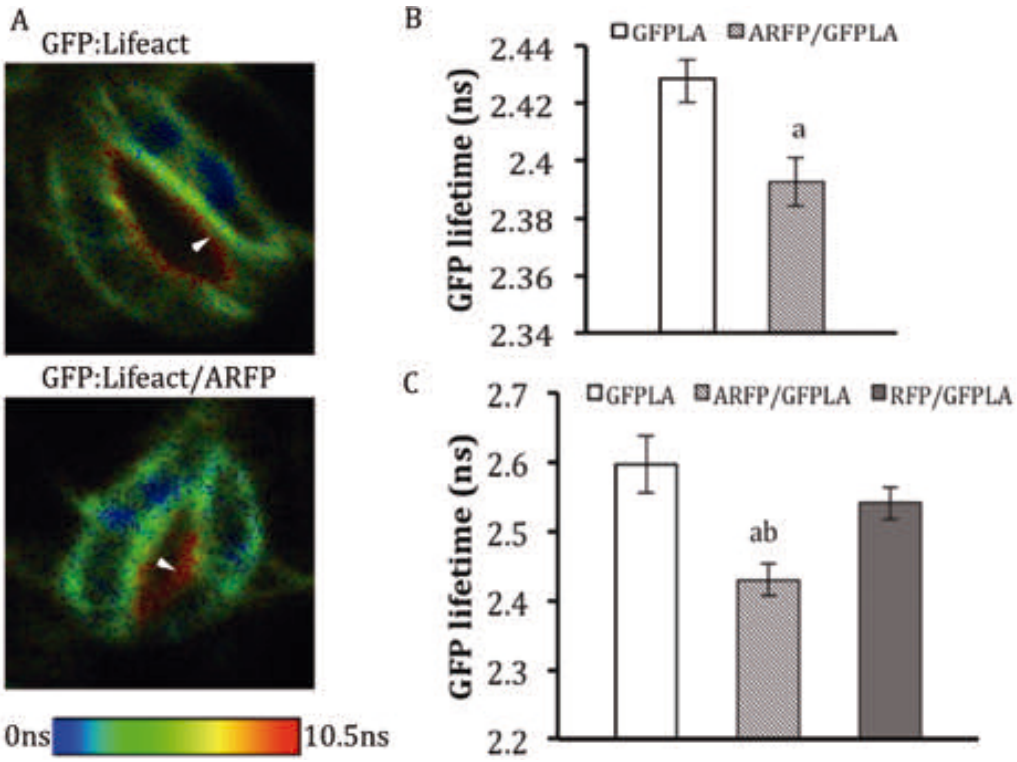
A
GFP:Lifeact
GFP:Lifeact/ARFP
0ns
10.5ns
B
GFPLA
ARFP/GFPLA
GFP lifetime (ns)
2.44
2.42
2.4
2.38
2.36
2.34
a
C
GFPLA
ARFP/GFPLA
RFP/GFPLA
GFP lifetime (ns)
2.7
2.6
2.5
2.4
2.3
2.2
ab

A *fba8-1*

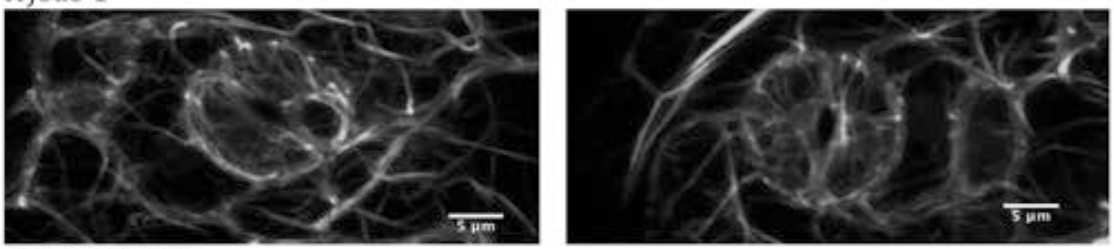

B aldolase:RFP

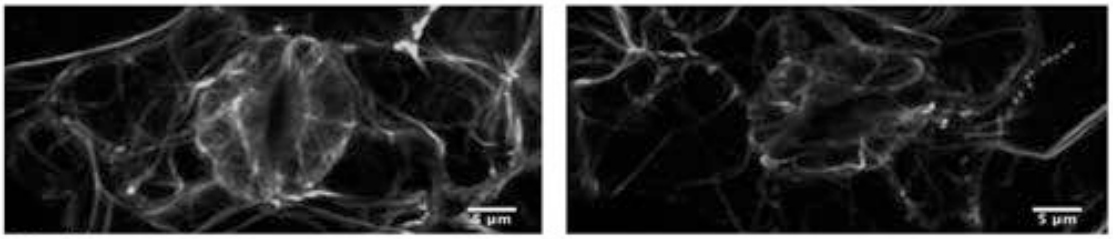

C Col-0

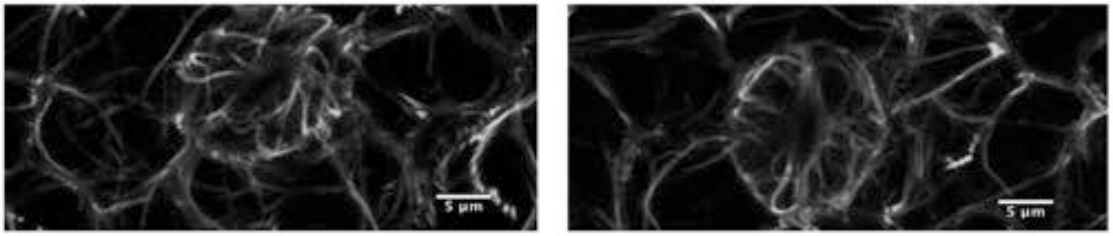

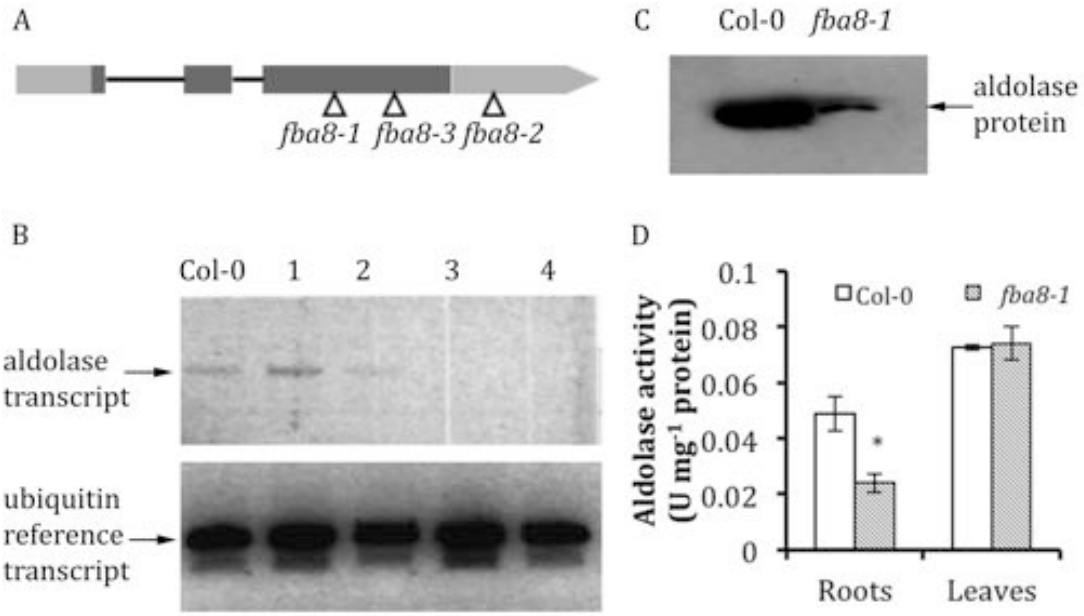
A
fba8-1 fba8-3 fba8-2
C
Col-0 fba8-1
aldolase protein
B
Col-0 1 2 3 4
aldolase transcript
ubiquitin reference transcript
D
Aldolase activity (U mg-1 protein)
0.1
0.08
0.06
0.04
0.02
0
Col-0
fba8-1
*
Roots
Leaves

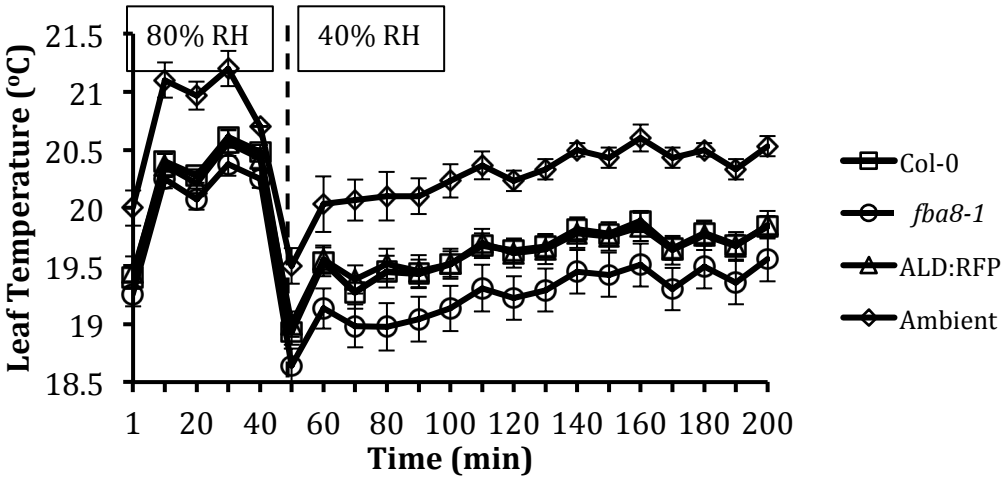
80% RH
40% RH
Leaf Temperature (°C)
21.5
21
20.5
20
19.5
19
18.5
1
20
40
60
80
100
120
140
160
180
200
Time (min)
Col-0
fba8-1
ALD:RFP
Ambient